A mathematical model to study railway track dynamics for the prediction of vibration levels generated by rail vehicles

J Otero, J Martínez, M A de los Santos and S Cardona

Proceedings of the Institution of Mechanical Engineers, Part F: Journal of Rail and Rapid Transit 2012 226: 62 originally published online 18 July 2011
DOI: 10.1177/0954409711406837

A mathematical model to study railway track dynamics for the prediction of vibration levels generated by rail vehicles

J Otero, J Martínez*, M A de los Santos, and **S Cardona**
Mechanical Engineering Department, Universitat Politècnica de Catalunya, Barcelona, Spain

The manuscript was received on 17 November 2010 and was accepted after revision for publication on 22 March 2011.

DOI: 10.1177/0954409711406837

Abstract: This article presents a mathematical model aimed at predicting wheel–rail contact vibration force arising from wheel profile irregularities. Prediction of vibrations caused by a passing train is a basic factor in environmental impact studies related to planning new railway lines. The prediction model is useful during the development of a project as it facilitates selection of the most suitable track for reducing vibration levels. This article presents the model, analyses the influence of the track base on the vibration-generating mechanisms, and compares the dynamic behaviour of the most widely used urban railway tracks.

Keywords: vibration predictions, wheel–rail contact, vibration level reduction

1 INTRODUCTION

The vibrations produced by a train passing along a railway track can cause problems in the immediate areas surrounding the track, as well as deterioration of the different parts making up the track. It is therefore useful to develop mathematical models which allow railway planners to analyse the dynamic behaviour of the track, and predict the vibration levels that may arise in the area.

The principal cause of vibrations when a train passes is the force fluctuations in the wheel-rail contact, derived from wheel profile irregularities. A mathematical model for the vibration-generating mechanism has been developed that allows us to predict, on the basis of irregularities in the wheel profiles, the vibratory response of the rail and wheel, as well as the contact forces generated in the wheel-rail interaction area [**1**]. Modelling includes the dynamic characteristics of the rail and carriage suspension, and uses Hertz's non-linear theory to characterize the wheel–rail contact. From the time history of the wheel–rail contact force, temporal registers are obtained from the vibration caused by the passing of a train wheel moving at a constant velocity along the track.

The vibration at a given point of the track is obtained through a convolution integral with variable kernel [**2**, **3**]. Therefore, it is necessary to find the impulse response of the track in terms of the distance between the chosen point of the track and the excitation point where the contact force is to be applied. The displacement of a point on the track is determined using the impulse response associated with track receptance. The vibration velocity at the same point of the track is determined by the impulse response associated with the track mobility. Both frequency responses are calculated for a frequency range of between 3 and 400 Hz. This range includes the frequencies of interest for studying vibrations caused by urban trains [**4**].

The model's development includes the analysis of the influence of slabs dynamic behaviour (slabs that act as a base for the track) on the vibration-generating mechanism. The results obtained from existing

**Corresponding author: Mechanical Engineering Department, Universitat Politècnica de Catalunya, Diagonal 647, 08028 Barcelona, Spain.*
email: jmartinez.miralles@upc.edu

intermediate slabs at various sections on Line 9 of the Barcelona suburban network are presented and compared with the results obtained when the track base is assumed to be fully rigid.

Finally, a comparative study of the vibratory behaviour of the most widely used urban railway tracks is presented. The results obtained with the proposed model are contrasted with experimental measurements.

2 VIBRATION GENERATION MODEL

This section presents the models for track, wheel, primary suspension, and contact force used in the vibration generation model.

2.1 Models of rails on rigid bases

Several authors [**2**, **3**, **5**, **6**] have proposed two different approaches for studying the vibratory behaviour of a railway track. Both approaches are based on the following assumptions: that the vibratory movement of both rails is independent, thus a single rail with its fastening elements is considered; that vibratory motion of the rail is vertical (as the study is limited to straight sections of track, and in this case, the force that is generated in the area of wheel–rail interaction is mainly vertical); and that the base of the track is considered rigid.

Both approaches model the rail as an infinite Euler–Bernoulli beam, and differ in their way of modelling the remaining elements of the track, such as fastenings, sleepers, ballast, and others. The first approach assumes that the dynamic parameters of these elements – inertia, stiffness, and damping – are uniformly distributed along the track. This approach is known as a *distributed parameter model*. The second approach treats the track elements as individual elements and introduces the actual separation between these elements. The inertia, stiffness, and damping parameters are thus distributed discretely along the track. This second approach is known as a *discrete parameter model*. Figure 1 provides an outline of the two models with the generalized coordinates and other variables used.

Both models provide equivalent results when the train speeds considered in the simulations are low (less than 100 km/h) [**2**, **3**], a condition that is met in urban and suburban railways.

2.2 Wheel and primary suspension model

The wheel, along with the rest of the unsprung mass, is modelled as a rigid body attached to the bogie *via* the primary suspension of the rail vehicle. This suspension is modelled using a spring–damper system. For the most relevant range of frequencies of vibrations generated by wheel–rail contact – between 10 and 200 Hz – it can be assumed that the sprung mass of the bogies and coach is not affected by the vibratory movement. The carriages are assumed to have two bogies, and the weight of the carriage distributed equally among the eight wheels.

2.3 Model of the normal wheel–rail contact force

The normal wheel–rail contact force, assumed to be vertical, is modelled using Hertz's non-linear theory. Figure 2 illustrates the interaction between the wheel and the rail, in which the wheel profile irregularity ε intervenes. If for one specific instant t, it is known the vertical displacement of the rail y_r at the contact point, the vertical position y_G of the wheel's centre and the value of its irregularity, the normal wheel–rail contact force F can be evaluated through the expression (1) [**1**, **7**].

$$F = \begin{cases} K_H \delta^{3/2} & \text{when } \delta = y_r - y_G + r - \varepsilon > 0 \\ 0 & \text{when } \delta = y_r - y_G + r - \varepsilon \leq 0 \end{cases} \quad (1)$$

With δ being the local deformation in the area of contact, r the radius of the wheel and K_H the non-linear contact stiffness, determined according to Hertz's

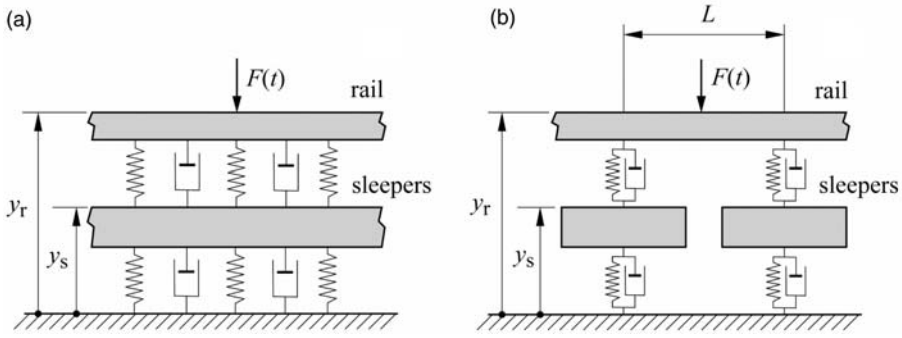

Fig. 1 Models of track with: (a) distributed parameters and (b) discrete parameters

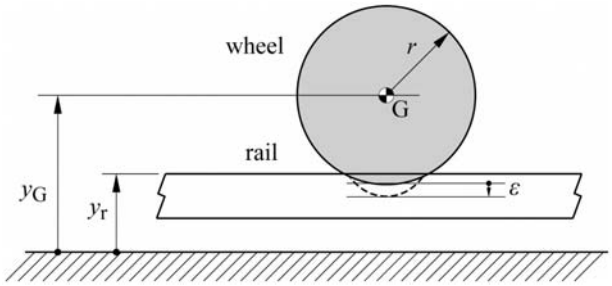

Fig. 2 Wheel–rail interaction for a profile irregularity of value ε

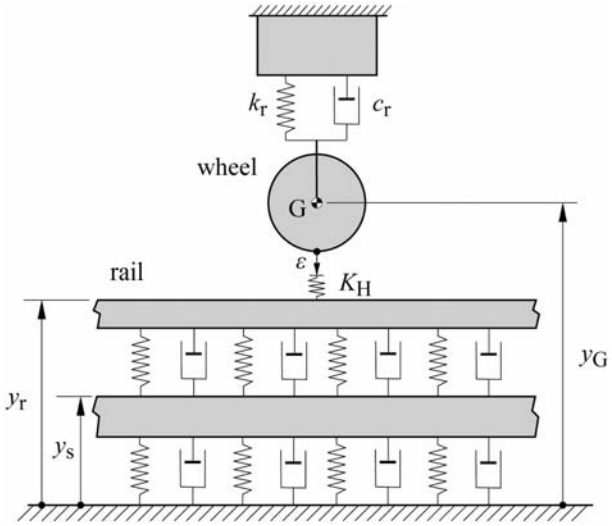

Fig. 3 Sketch of the global model of vibration generation, using the distributed parameters model

theory. The profile irregularity ε is described in terms of the wheel perimeter, and introducing its rotation speed, in terms of time. When $\varepsilon < 0$, the irregularity of the profile is towards the centre of the wheel, and when $\varepsilon > 0$, the irregularity is outward. Figure 3 shows the sketch of the global model of generation combining the three models described in this section.

3 INFLUENCE OF THE DYNAMIC BEHAVIOUR OF THE TRACK BASE IN THE VIBRATION-GENERATING MECHANISM

In order to analyse the influence of the track base's dynamic behaviour on the vibration-generating mechanism, the base has been modelled as a concrete slab. The slab has been characterized in the model by means of its receptance. The case of intermediate slabs in various sections of Line 9 of the suburban Barcelona Metropolitan Rail Network – FMB – has been studied. The results obtained for the studied case are presented and compared to results obtained when the track base is assumed to be fully rigid.

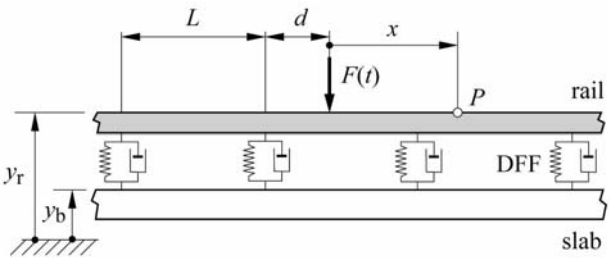

Fig. 4 Discrete model of a DFF track installed over an intermediate concrete slab

3.1 Vertical motion equation of the rail

The discrete parameters track model was used to find the vertical motion equation of the rail, as this model permits introduction of the point receptance of the slab. Figure 4 describes the configuration of a discrete direct fixation fastening (DFF) track supported by an intermediate concrete slab. This type of track is used in several sections of the FMB Line 9. The discrete receptance of each fastening is combined with the receptance of the slab at the point where each fastening is located.

Track receptance – defined as the relation between the vertical displacement of the rail at point P and a vertical excitation force applied to the rail at the same or different point – is derived from the equation (2). This in turn corresponds to the vertical motion equation of the rail, valid for a stationary regime, when the excitation force is a harmonic force of frequency $f = \omega/2\pi$.

$$E\,I(1+\mathrm{j}\,\mu)\,\frac{\partial^4 \tilde{y}_r}{\partial x^4} + \rho\,S\,\omega^2\,\tilde{y}_r = -\tilde{F}\,\delta(x) + \sum_{n=-\infty}^{\infty} \tilde{F}_{DFF}\,\delta(x - n\,L + d) \quad (2)$$

with $F = \tilde{F}\,e^{\mathrm{j}\,\omega t}$; $y_r = \tilde{y}_r\,e^{\mathrm{j}\,\omega t}$

x is the longitudinal coordinate, $\tilde{F}$ the phasor of the harmonic excitation force F, $\tilde{y}_r$ the phasor of the vertical displacement y_r at point P, E the Young's modulus of the rail material, I the second-order momentum of the area of the rail section, S the rail section, ρ the density of the rail, μ the rail's structural damping factor, L the distance between fastenings, d the distance between the point of application of force and the nearest fastening, F_{DFF} the force that each fastening exerts on the rail, and $\delta(x)$ the Dirac Delta function.

The force exerted by a fastening can be expressed as a function of the rail displacement by means of the fastening's receptance, R_{DFF}. The expression (3) describes this relationship. Upon substituting the expression (3) in equation (2), the equation (4) is

obtained, which corresponds to the motion equation in the frequency domain.

$$\tilde{F}_{\mathrm{DFF}} = \frac{\tilde{y}_{\mathrm{r}}}{R_{\mathrm{DFF}}} \tag{3}$$

$$E\,I(1+\mathrm{j}\,\mu)\frac{\partial^4 \tilde{y}_{\mathrm{r}}}{\partial x^4} - \left(\rho\,S\,\omega^2 + \frac{1}{R_{\mathrm{DFF}}}\sum_{n=-\infty}^{\infty}\delta(x-n\,L+d)\right)\tilde{y}_{\mathrm{r}} = -\tilde{F}\,\delta(x) \tag{4}$$

The receptance of a fastening is obtained from its stiffness k_{DFF}, from its hysteretic damping factor μ_{DFF}, and from the slab receptance R_{b}, according to the expression (5).

$$R_{\mathrm{DFF}} = -\frac{\left(k_{\mathrm{DFF}}(1+\mathrm{j}\,\mu_{\mathrm{DFF}})R_{\mathrm{b}}+1\right)}{k_{\mathrm{DFF}}(1+\mathrm{j}\,\mu_{\mathrm{DFF}})} \tag{5}$$

The receptance of the intermediate slab is determined by means of the superposition of flexural vibration modes of a finite rectangular slab clamped at two opposite sides and free at the other two sides [**8**, **9**]. The expression (6) describes the slab receptance, in which ω_i and $\Phi_i(\mathrm{P})$ represent, respectively, the natural angular frequency and the displacement of point P of the slab associated to its mode i, m_{b} the total mass of the slab, α_i the normalization factor of the mode i, and μ_{b} the damping factor of the slab.

$$R_{\mathrm{b}}(\omega) = \frac{1}{m_{\mathrm{b}}}\sum_{i=1}^{\infty}\frac{\Phi_i^2(\mathrm{P})}{\alpha_i\left(\omega_i^2(1+\mathrm{j}\,\mu_{\mathrm{b}})-\omega^2\right)} \tag{6}$$

3.2 Application in the case of Line 9 of the Barcelona metro

A tubular tunnel was built over various sections of Line 9 of the FMB, with an intermediate 0.4 m thick slab of reinforced concrete separating the tracks in either direction. As shown in Fig. 5, the slab is discontinuous, and consists of 20 m long sections clamped at their sides to the wall of the tunnel. The track uses DFF fastenings to hold each rail to the slab. The parameters of the slab and DFF fastenings, provided by the manufacturers, are set out in Appendix 2.

This section analyses slab vibratory behaviour in the mechanism of vibration generation and transmission using the model set out in Section 3.1. The determination of the intermediate slab's vibration modes lets us characterize its receptance according to equation (6). The modes considered have been obtained from a finite element model [**10**]. The first eight slabs' bending modes have been considered: two with purely longitudinal nodal lines and six with longitudinal and transverse nodal lines, all of which are contained in the frequency range of interest. Figure 6 shows the shape of the two longitudinal modes. Higher frequency modes are not considered because of their negligible contribution to the slab's vibration response.

To obtain slab receptance, it is assumed that the eight modes contribute to the modal superimposition with their maximum amplitude. This provides a unreal situation that is more unfavourable than any real situation in which the modes are superimposed with the amplitudes corresponding to the locations studied. These are the locations where the rails are attached. Figure 7 shows the calculated receptance.

Introducing the vertical receptance of slab into equations (4) and (5), global receptance of DFF track has been determined at the midpoint of the rail between two fastenings with force F applied at the same point. Figure 8 shows this receptance and also that obtained when the base is considered rigid, i.e. when the receptance is $R_{\mathrm{b}}(\omega) = 0$.

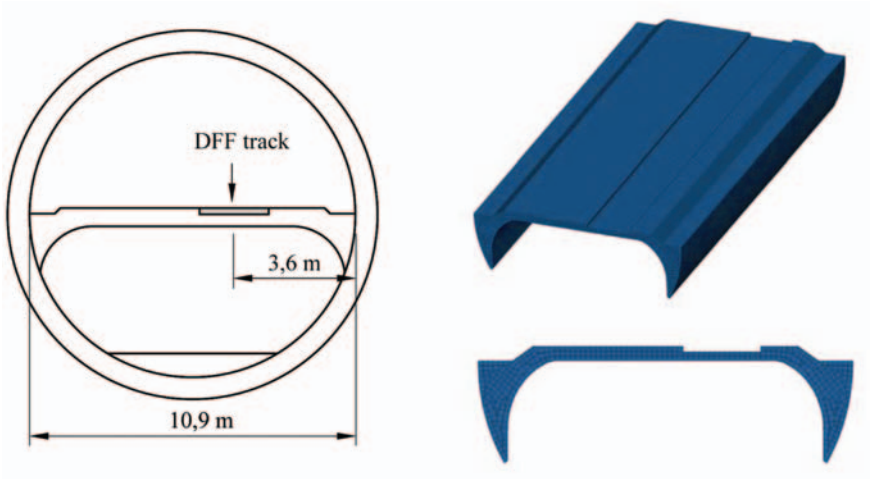

Fig. 5 Cross-section of the tunnel and shape of the intermediate concrete slab of the FMB Line 9

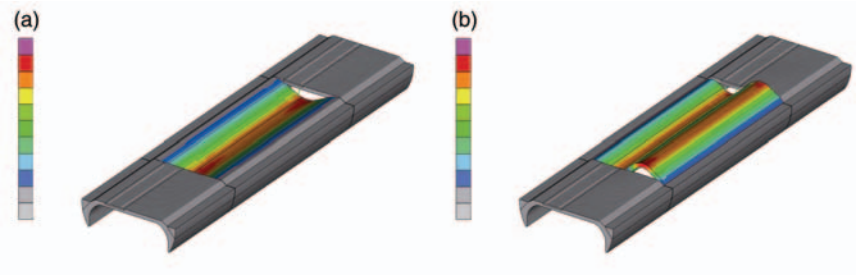

Fig. 6 Longitudinal modes of the intermediate slab: (a) first mode (23 Hz) and (b) seventh mode (52.3 Hz)

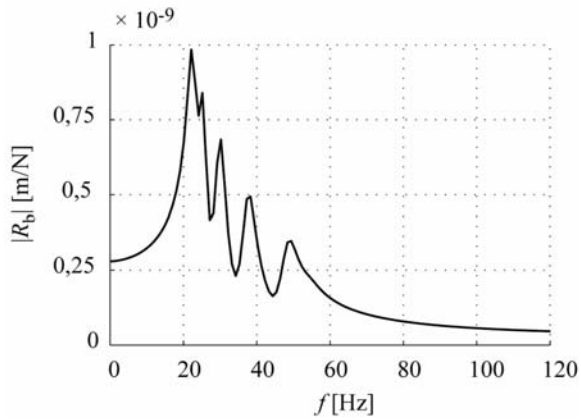

Fig. 7 Vertical receptance of the slab obtained through superimposing its first eight modes

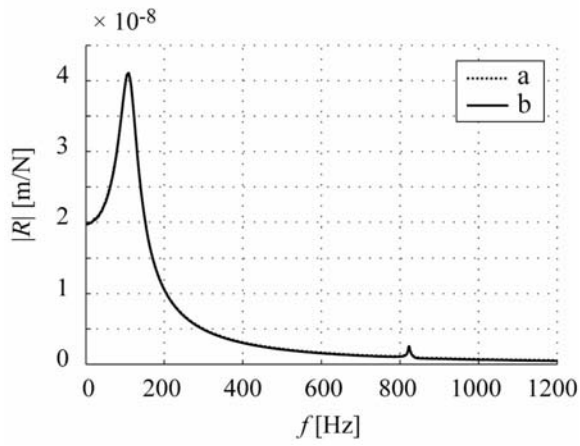

Fig. 8 Comparison of the vertical receptance of the track: (a) rigid base, (b) considering the receptance of the intermediate slab. There are not significant differences between them

Comparison of both receptances clearly shows that the dynamics of the intermediate concrete slab have virtually no effect on vertical track receptance, and therefore on the mechanism of vibration generation. In conclusion, the rigid base hypothesis considered in the track model is valid for the studied slab and also for any kind of concrete base of equal or greater thickness.

4 DETERMINING RAIL VIBRATION VELOCITY. EXPERIMENTAL VALIDATION

With the aim of validating the model, the vibration velocity is determined at a fixed point on the rail, as experimental measurements of the rail's vertical vibration velocity are available.

The rail's vibration velocity, $\dot{y}_r(t)$, is determined by means of the convolution integral between the track's impulse response $h(t)$ and the fluctuating value of the wheel–rail contact force $F(t)$ obtained from the numerical resolution of the equation system of the generation model. The distributed parameter model is considered, whose formula is simpler than that of the discrete parameter model. The expression (7) describes the convolution integral.

$$\dot{y}_r(t) = \int_0^t h(t-\tau)F(\tau)\mathrm{d}\tau \tag{7}$$

The impulse response is obtained as the Inverse Fourier Transform of the cross-mobility of the track $M(\omega)$ described in equation (8). This mobility relates the rail's vertical velocity at one point and the contact force applied to the rail at either the same or a different point.

$$M(\omega) = \mathrm{j}\omega\, R(\omega) \tag{8}$$

The impulse response acts as the convolution kernel and varies at each stage of integration due to the displacement of the contact force along the rail. In this way, the train's speed can be introduced into the model [**2**, **3**].

The obtained results correspond to a classic track with ballast, assuming that an 800 mm diameter wheel with severe profile irregularity, which was obtained experimentally, is moving along the rail [**11**]. The wheel had been in service for a long

period of time and was in the maintenance department of FMB to be machined. The profile irregularity was obtained using the wheel machining lathe as test rig and linear variable differential transformer sensors to register the profile. Four different profiles of four tread perimeters were registered, and the rolling perimeter of the wheel on a straight track was chosen. Figure 9 shows this profile as a function of wheel's perimetrical coordinate p. The parameters of the studied track are gathered in Appendix 2.

Figure 10 shows the contact force obtained with the profile irregularity in Fig. 9. It can be seen that the contact force – which sometimes vanishes–oscillates around its mean value $F_0 = 61$ kN. This mean value is due to the load on the wheel and its own weight. A train speed of $v = 18$ m/s is assumed in order to obtain this result.

Finally, Fig. 11(a) shows the vibration velocity obtained at a point on the rail in the case of a passing two-wheeled bogie with profile, as shown in Fig. 9. Vibration velocity is obtained by superimposing the vibrations produced by each of the wheels. Figure 11(b) shows the measured vibration velocity of a passing train bogie on Line 3 of the FMB. The measurements were taken of a track with ballast and wheels with similar wear patterns to that of the simulated wheel. Comparison of the two results shows a good similarity in terms of vibration magnitude and passing duration.

Figure 12 shows the same comparison in the frequency domain. The graph shows the energy spectrum of rail vertical vibration velocity, expressed in 1/3 octave bands, for both time histories in Fig. 11. The graph further reveals similar results in the two cases, despite differences in wheel profile and track parameters of the calculated and the measured bogie passing.

5 PERFORMANCE ANALYSIS OF DIFFERENT TYPES OF TRACK

Using the vibration generation model presented in Section 2, the vibratory behaviour of various types of track used in the suburban network of the FMB has been studied. In this way, the usefulness of the model for selecting the most appropriate track types to reduce vibration levels, and for adjusting their

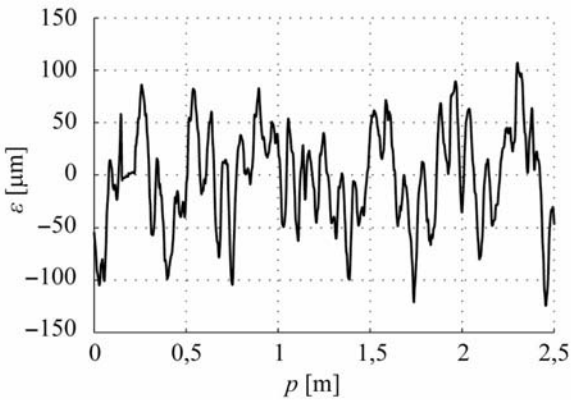

Fig. 9 Profile irregularity of the chosen wheel as a function of its perimetrical coordinate p

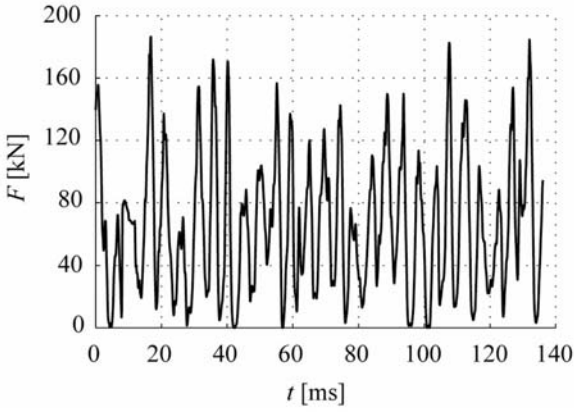

Fig. 10 Wheel-rail contact force calculated from the wheel profile irregularity in Fig. 9. Assumed velocity $v = 18$ m/s

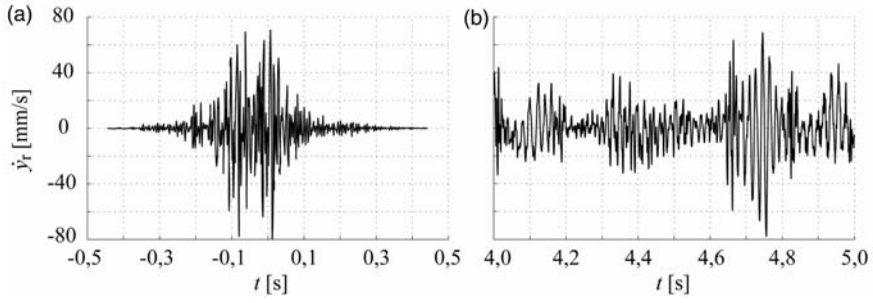

Fig. 11 Rail vertical vibration velocity of the rail: (a) calculated from the profile irregularity in Fig. 9 and (b) obtained experimentally

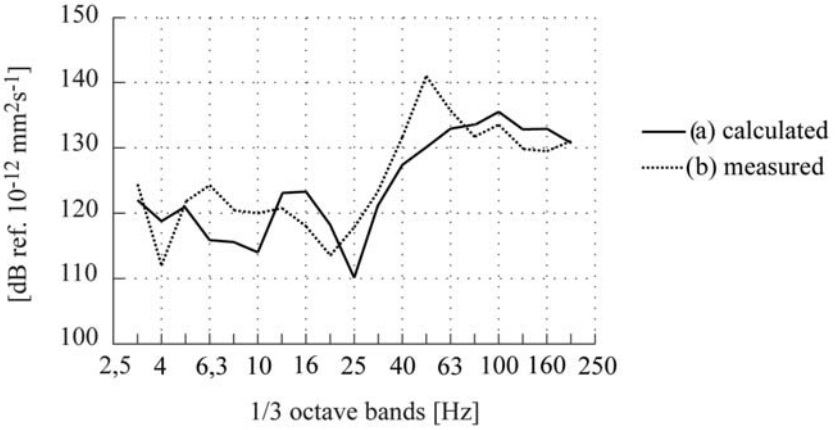

Fig. 12 Energy spectrum of the vertical vibration velocity of the rail, for 1/3 octave bands from 3.15 to 200 Hz obtained from: (a) time history in Fig. 11(a) and (b) time history in Fig. 11(b)

parameters, can be demonstrated. Five types of track have been analysed with regard to inertia, stiffness, and damping (listed in Appendix 2). The tracks studied are:

(a) classic track, with ballast and concrete sleepers;
(b) bi-block track;
(c) IPA system track. Track consisting of prefabricated slabs on an asphaltic concrete layer. Rails are attached to the slabs by means of elastic fixations;
(d) floating slab track;
(e) track with DFF fastenings, without sleepers.

Track parameters have been obtained from manufacturers and references. The inertia parameters of rails, sleepers, concrete blocks, and slabs are easily obtained from the density and geometry of these elements. Stiffness and damping factors of rail pads and elastic layers are supplied by manufacturers and the technical staff of FMB. These parameters are usually obtained by means of experimental tests to assess the dynamic stiffness and loss factor from the relationship between applied force and elongation at several test frequencies. Finally, ballast parameters are taken from several authors in references [**7**, **12**].

The behaviour of each track has been characterized by means of the magnitude of the wheel–rail contact force and the track reduction level, A. This reduction level is defined as the relation between the level of the rail's vertical vibration velocity, $\dot{y}_{\mathrm{r\,RMS}}$, and the level of vertical vibration velocity at the base of the track $\dot{y}_{\mathrm{bRMS}}$. Expression (9) shows the definition of the reduction level.

$$A = 20 \lg \frac{\dot{y}_{\mathrm{r\,RMS}}}{\dot{y}_{\mathrm{b\,RMS}}} \tag{9}$$

$\dot{y}_{\mathrm{b\,RMS}}$ is obtained from the force transmitted at the base of the track, assuming that this concrete base on the ground will behave as a propagatory medium of constant impedance, as described by the expression (10)

$$Z_{\mathrm{b}} = 8\left(\frac{E_{\mathrm{b}} I_{\mathrm{b}} \rho_{\mathrm{b}} h_{\mathrm{b}}}{1-\upsilon_{\mathrm{b}}^2}\right)^{1/2} \quad \text{with } I_{\mathrm{b}} = \frac{h_{\mathrm{b}}^3}{12} \tag{10}$$

where ρ_{b}, E_{b}, υ_{b} are, respectively, the density, the elasticity modulus, and the Poisson ratio of the concrete, and h_{b} the thickness of the base [**9**].

The contact force, the force transmitted at the base of the track, and the rail's vertical vibration were obtained from the numerical resolution of the equation system of the generation model, as described in Section 2, assuming that a wheel passed over the rail, at $v = 18$ m/s, with the real profile irregularity shown in Fig. 9.

The results obtained for the five track types are shown in Table 1 and Fig. 13. The table shows the values of the contact force and the reduction level for each type of track for the frequency band B from 10 to 125 Hz. In Fig. 13, the reduction level is shown for 1/3 octave bands included in the frequency band B.

The results clearly demonstrate that, as is well-known, the floating slab track is the best performing

Table 1 Values of contact forces, F_{RMS}, and reduction levels, A_{B} for the five track types analysed

Type of track	F_{RMS} (kN)	A_{B} (dB)
Classic track, with ballast	43.7	45.1
Bi-block track	42.1	40.8
IPA system track	36.9	47.9
Floating slab track	32.6	65.4
DFF track	43.6	37.4

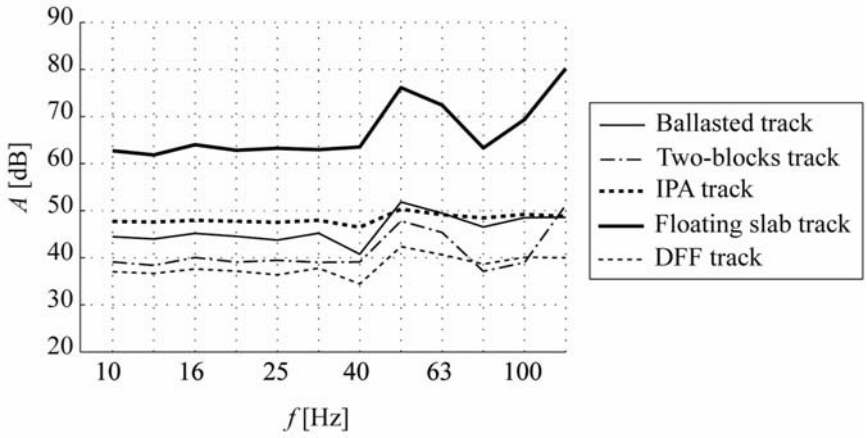

Fig. 13 Comparison of the rail-base reduction level, in 1/3 octave bands, for different types of track

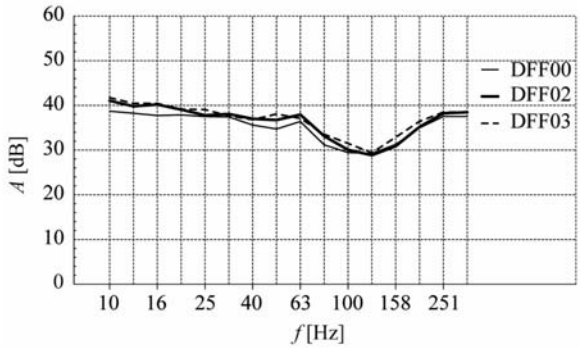

Fig. 14 Rail-base reduction level obtained experimentally for a track with DFF fastenings

of all the track types studied. This is evident in Table 1, which shows that for this type of track, the vibration reduction level is the greatest and the contact force the lowest. The other types of track show reduction levels between 35 and 50 dB, with the bi-block track and the DFF track showing the lowest levels. However, the DFF track allows for lower tunnel heights, and the bi-block track is suitable for many sections where requirements are not very high in terms of the track's vibratory behaviour.

Comparison of the different types of track performance shows a good agreement with the recommendations suggested in international standards in terms of the anti-vibratory characteristics of the tracks analysed [**13**].

With the aim of validating the model yet again, the results obtained for reduction levels of a track with DFF fastenings were compared with results obtained experimentally on a section of Line 11 of the FMB, where this type of fastening is used. The experimental results are shown in Fig. 14 and correspond to three types of fastening with elastomer pads of slightly different stiffness, identified as DFF00, DFF02, and DFF03. The results were obtained by measuring the vertical vibration velocity at the rail and at the base of the track as a test train passed over.

Comparing the reduction levels shown in the Figs 13 and 14, it is clear that the reduction level results obtained from the model are similar to the experimental results obtained for the three types of elastomer under study.

6 CONCLUSIONS

This study shows that intermediate slab vibratory behaviour – slab used as a track base in some sections of Line 9 of the Barcelona metro network – has no effect on the vibration-generation mechanism. Therefore, the hypothesis of the rigid base is valid, and can be extrapolated to concrete bases used in tunnel construction that are heavier and stiffer than intermediate slabs.

The model facilitates assessment of wheel–rail contact force and vibration reduction levels. Both magnitudes are necessary for evaluating anti-vibratory track performance.

The results obtained from the model, the level of the rail's vibration velocity, and the reduction level between the rail and the track base are similar to the experimental results for the studied frequencies.

The vibration-generation model here presented proved useful in predicting the influence of inertia, stiffness, and damping parameters on the vibratory behaviour of different types of track. This model can therefore be used in the project and development stages of new railway infrastructures.

FUNDING AND ACKNOWLEDGEMENTS

The study presented in this article would not have been possible without the financial support

of the Catalan government's public company 'Infraestructuras Ferroviarias de Catalunya' (IFERCAT), provided as part of the IFERCAT-UPC agreement for the environmental impact study of vibrations in Line 9 of the FMB's suburban network.

Similarly, the authors thank Transports Metropolitans de Barcelona (TMB), the managing company of Ferrocarrils Metropolitans de Barcelona (FMB), for their support in permitting access to their installations and facilitating the taking of measurements and experiments on real sections of track, with trains in service as well as test trains.

Finally, the authors thank the research group of the Laboratory of Acoustic and Mechanical Engineering (LEAM) in the Mechanical Engineering Department of the Universitat Politècnica de Catalunya (UPC), for their participation in the IFERCAT-UPC agreement and the FEM analysis of the intermediate slab used in this study.

REFERENCES

1 **Otero, J., Martínez, J., de Los Santos, M. A.,** and **Cardona, S.** Study of the vibrations generated by the passage of a train. A wheel-track system modelization. In Proceedings of the 10th International Research/ Expert TMT 2006 Conference, Lloret de Mar, Barcelona, Spain, 11–15 September 2006, pp. 1403–1406.

2 **de Los Santos, M. A., Martínez, J.,** and **Cardona, S.** A convolution application to determine the dynamic response of a railway track. *Mech. Syst. Sig. Process.*, 1995, **9**(6), 707–708.

3 **Martínez, J., de los Santos, M. A.,** and **Cardona, S.** A convolution method to determine the dynamic response in a railway track submitted to a moving vertical excitation. *Machine Vibration*, 1995, **4**, 142–146.

4 Noise and vibration from railway vehicles. In *Handbook of Railway Vehicles Dynamics* (Ed. S. Iwnicki), 2006, ch. 10, pp. 279–325 (Taylor & Francis, Boca. Raton, USA) ISBN: 0-8493-3321-0.

5 **Grassie, S. L., Gregory, R. W., Harrison, D.,** and **Johnson, K. L.** The dynamic response of railway track to high frequency vertical excitation. *Proc. IMechE Part C: J. Mech. Eng. Sci.*, 1982, **24**(2), 77–90.

6 **Johansson, A.** and **Nielsen, J. C. O.** Out-of-round railway wheels – wheel-rail contact forces and track response derived from field tests and numerical simulations. *Proc. IMechE, Part F: J. Rail and Rapid Transit*, 2003, **217**, 135–146.

7 **Wu, T. X.** and **Thompson, D. J.** A hybrid model for the noise generation due to railway wheel flats. *J. Sound Vib.*, 2002, **251**(1), 115–139.

8 **Leissa, A. W.** Rectangular Plates. In *Vibration of plates*, 1993, ch. 4, pp. 41–45 (NASA; published by the Acoustical Society of America) ISBN: 1-56396-294-2.

9 **Benassi, L.** and **Elliot, S. J.** The equivalent impedance of power-minimising vibration controllers on plates. *J. Sound Vib.*, 2005, **283**(12), 47–67.

10 **Otero, J., Martínez, J.,** and **de los Santos, M. A.** Evaluación de las vibraciones generadas al paso de un tren considerando diferentes tipologías de vía. In Proceedings of the 9th Congreso Iberoamericano de Ingeniería Mecánica. Las Palmas de Gran Canaria, Spain, 17–19 November 2009, pp. 1403–1406.

11 **Fernández-Díaz, E.** *Contribució a l'estudi de la detecció i l'anàlisi de les vibracions produïdes pels bogis d'un ferrocarril.* PhD Thesis, (written in catalan), Universitat Politècnica de Catalunya (UPC), Spain, 2000, pp. 138–154.

12 **Nielsen, J. C. O.** and **Fredö, C. R.** Multi-disciplinary optimization of railway wheels. *J. Sound Vib.*, 2006, **293**(3–5), 510–521.

13 **ISO 14837–1.** Mechanical vibration. Ground-borne noise and vibration arising from rail systems. Part 1: General guidance, 2005.

APPENDIX 1

Notation

A	reduction level of vibration
d	distance between the force application point and the nearest fastening
E	Young's modulus of the rail material
E_b	Young's Modulus of concrete
f	frequency
F	wheel–rail contact force; excitation force
F_{DFF}	force that each fastening exerts on the rail
F_0	mean value of the contact force
$\tilde{F}$	phasor of the harmonic excitation force F
h	track's impulse response
h_b	thickness of the slab; thickness of the track base
I	second-order momentum of the area of the rail section
k_{DFF}	fastening's stiffness
K_H	non-linear contact stiffness
L	distance between fastenings
m_b	total mass of the slab
M	track's mobility
p	perimetrical coordinate of the wheel
r	wheel radius
R	track's receptance
R_b	slab's receptance
R_{DFF}	fastening's receptance
S	rail section
v	train speed
x	longitudinal coordinate
y_b	slab vertical displacement; track base vertical displacement
y_G	vertical position of the wheel's centre
y_r	rail vertical displacement
y_s	sleepers vertical displacement

$\tilde{y}_r$	phasor of the rail vertical displacement y_r
$\dot{y}_b$	vertical vibration velocity of the track base
$\dot{y}_r$	vertical vibration velocity of the rail
Z_b	track base impedance
α_i	normalization factor of the i slab's mode
δ	Dirac Delta function
ε	wheel profile irregularity
μ	rail's structural damping facto
μ_b	structural damping factor of concrete
μ_{DFF}	hysteretic damping ratio of a fastening
υ_b	Poisson's ratio of concrete
ρ	density of the rail material
ρ_b	density of concrete
$\Phi_i(P)$	displacement of point P associated to its mode i
ω	angular frequency
ω_i	natural angular frequency of the i slab's mode

APPENDIX 2

Parameters used in the simulations

Parameters of the intermediate concrete slab

Thickness of the slab (h_b)	0.4 m
Young's Modulus of concrete (E_b)	27.6 GPa
Density of concrete (ρ_b)	2400 kg/m^3
Poisson's ratio of concrete (υ_b)	0.175
Damping factor of concrete (μ_b)	10%

Parameters of rail UIC 54

Distributed mass of rail UIC 54	54.4 kg/m
Transversal section of rail (S)	6930 mm^2
Inertia of rail (I)	23.5×10^6 mm^4
Young's Modulus of rail (E)	210 GPa
Density of rail (ρ)	7850 kg/m^3
Damping factor of rail (μ)	2%

Parameters of the different types of track

Model of distributed parameters.
Assumed distance between sleepers or fastenings, $L = 0.6$ m.

Conventional track with ballast	
Stiffness under rail	Rigid
Stiffness of ballast	83.3 (MN/m)/m
Damping factor under rail	Rigid
Damping factor of ballast	40%
Distributed mass of sleepers	270 kg/m
Bi-block track	
Stiffness under rail	Rigid
Stiffness under blocks	29.3 (MN/m)/m
Damping factor under rail	Rigid
Damping factor under blocks	20%
Distributed mass of concrete blocks	158 kg/m
IPA system track	
Stiffness under rail	68 (MN/m)/m
Stiffness of the layer under slab	65 (MN/m)/m
Damping factor under rail	30%
Damping factor of the layer under slab	10%
Distributed mass of prefabricated slab	900 kg/m
Floating slab track	
Stiffness under rail	150 (MN/m)/m
Stiffness of elements under slab	130 (MN/m)/m
Damping factor under rail	40%
Damping factor of elements under slab	10%
Distributed mass of floating slab	3000 kg/m
DFF track without sleepers	
Stiffness of fastenings	32.5 (MN/m)/m
Damping factor of fastenings	40%